AD-A042 211 NAVAL RESEARCH LAB WASHINGTON D C F/G 20/6
AN INVESTIGATION OF 10 TO THE 12TH POWER W PER SQ CM FOCUSED RE--ETC(U)
MAY 77 D J JOHNSON, D J NAGEL, W F OLIPHANT

UNCLASSIFIED NRL-MR-3521 NL

| OF |
AD
A042211

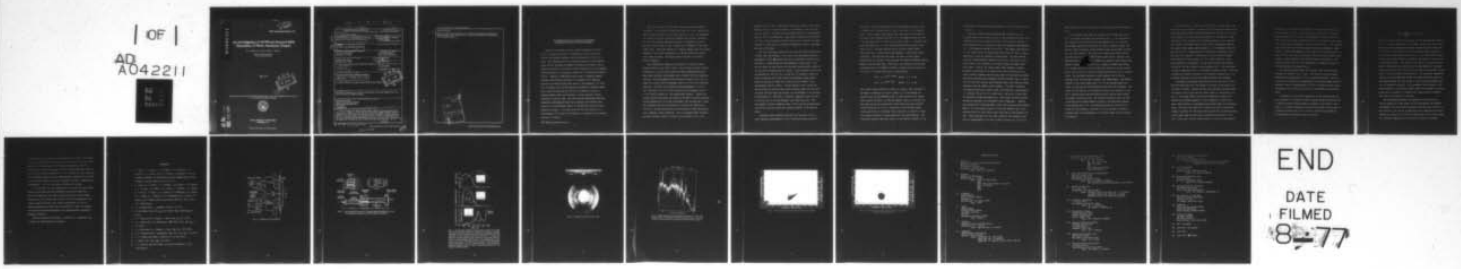

END

DATE
FILMED
8-77

12

NRL Memorandum Report 3521

An Investigation of 10^{12}W/cm^2 Focused REB Deposition of Thick Aluminum Targets

D. J. JOHNSON, D. J. NAGEL, and W. F. OLIPHANT

Plasma Technology Branch
Plasma Physics Division

May 1977

This research was sponsored by the Defense Nuclear Agency under subtask T99QAXLA014, work unit 05, work unit title Advanced Concepts.

NAVAL RESEARCH LABORATORY
Washington, D.C.

10 to the 12th power W/sq cm

per

SECURITY CLASSIFICATION OF THIS PAGE (When Data Entered)

REPORT DOCUMENTATION PAGE	READ INSTRUCTIONS BEFORE COMPLETING FORM
1. REPORT NUMBER: NRL Memorandum Report 3521	2. GOVT ACCESSION NO. / 3. RECIPIENT'S CATALOG NUMBER
4. TITLE (and Subtitle): AN INVESTIGATION OF 10^{12} W/cm^2 FOCUSED REB DEPOSITION OF THICK ALUMINUM TARGETS.	5. TYPE OF REPORT & PERIOD COVERED: Interim report on a continuing NRL problem
	6. PERFORMING ORG. REPORT NUMBER
7. AUTHOR(s): D.J. Johnson, D.J. Nagel, and W.F. Oliphant	8. CONTRACT OR GRANT NUMBER(s)
9. PERFORMING ORGANIZATION NAME AND ADDRESS: Naval Research Laboratory, Washington, D.C. 20375	10. PROGRAM ELEMENT, PROJECT, TASK AREA & WORK UNIT NUMBERS: NRL Problem H02-26A, Project DNA T99QAXLA014
11. CONTROLLING OFFICE NAME AND ADDRESS: Defense Nuclear Agency, Washington, D.C. 20305	12. REPORT DATE: May 1977
	13. NUMBER OF PAGES: 23
14. MONITORING AGENCY NAME & ADDRESS(if different from Controlling Office): 21p.	15. SECURITY CLASS. (of this report): UNCLASSIFIED
	15a. DECLASSIFICATION DOWNGRADING SCHEDULE
16. DISTRIBUTION STATEMENT (of this Report): Approved for public release; distribution unlimited. NRL-MR-3521	
17. DISTRIBUTION STATEMENT (of the abstract entered in Block 20, if different from Report)	
18. SUPPLEMENTARY NOTES: This research was sponsored by the Defense Nuclear Agency under subtask T99QAXLA014, work unit 05, work unit title Advanced Concepts.	
19. KEY WORDS (Continue on reverse side if necessary and identify by block number): Focused electron beam; Relativistic electron beam deposition; Electron beam target interactions; VUV-radiation; Accelerated ions	

MA/sq cm micrometer

20. ABSTRACT (Continue on reverse side if necessary and identify by block number)

The VUV-emission from 6061-T6 aluminum targets, exposed to an intense focused electron beam, and ions accelerated to the diode potential were examined to study the electron absorption mechanism for a 1 meV electron beam with current density of 1 MA/cm^2. The VUV-emission was observed with aluminum cathode x-ray diode operated with and without 1/2 μm aluminum filters and a near normal incidence grating spectrograph. Carbon ions were observed with a Thomson mass spectrograph and their charge state used to estimate the anode plasma temperature. The VUV-

→ next page

(Continues)

DD FORM 1 JAN 73 1473 EDITION OF 1 NOV 65 IS OBSOLETE S/N 0102-014-6601

SECURITY CLASSIFICATION OF THIS PAGE (When Data Entered)

251 950

Abstract (Continued)

cont

emission and carbon charge states observed are consistent with classical electron deposition and indicate an anode surface temperature of a few eV with the peak temperature occurring at the time of impedance collapse.

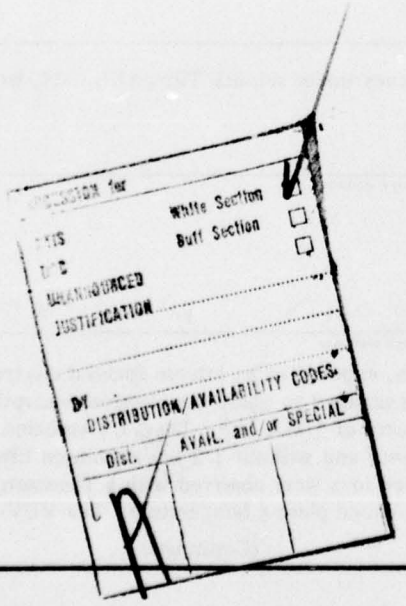

AN INVESTIGATION OF 10^{12}W/cm^2 FOCUSED REB DEPOSITION OF THICK ALUMINUM TARGETS

Recently the concept of using a pulsed relativistic electron beam[1,2] to implode and ignite a thermonuclear fusion pellet has received considerable attention as an alternative to the use of a laser. This approach would be considerably enhanced if the electron range could be shortened by anomalous absorption processes, such as enhanced deposition in the anode blow-off material due to self-magnetic field penetration[3] or increased coupling due to beam-plasma instabilities[2,4]. Analysis of REB-induced shock waves in aluminum targets[5] indicated that electron deposition is consistent with classical processes for electron beam power levels of approximately 10^{11} W/cm^2. Here we examine the electron absorption mechanism at somewhat higher power levels by measuring the VUV- and ion emission from thick aluminum targets under the influence of a high intensity focused relativistic electron beam. The data obtained demonstrate that time integrated spectrographic data must be analyzed with extreme care because of the preponderant amount of VUV-emission during the diode impedance collapse. It is also shown that at power levels up to approximately 10^{12} W/cm^2 the VUV-emission is consistent with classical absorption processes.

Note: Manuscript submitted May 10, 1977.

Data were obtained with the Naval Research Laboratory Gamble II generator[6], which supplied an electrical pulse of 60 nsec duration with peak corrected voltage of 1.2 MV and current of 0.6 MA. The generator was operated in reverse (positive) polarity which allowed convenient access to the electron beam target (anode) for diagnostic purposes. The diode used is shown in Fig. 1 along with a schematic of the diagnostics used. The diode utilized a 3° tapered cathode with 40 mm inside diameter, 80 mm outside diameter and 2.7 mm gap between the cathode inside edge and anode. The planar anodes used were 1.6 cm thick 6061-T6 aluminum.

The VUV-radiation diagnostics consisted of an array of three aluminum cathode x-ray diodes[7] (XRD's) which yielded the time resolved VUV-emission in three proton energy bands and a McPherson Model 225 near normal incidence spectrograph which observed the time integrated spectrum. The spectrograph recorded emission between 4 and 12 eV, on Kodak 101-01 film, with a wavelength window of 60 nm for an individual data shot. The XRD's were sensitive from approximately 5 to 25 eV when unfiltered, 20 to 80 eV when filtered by $\frac{1}{2}$ μm aluminum, and 150 to 280 eV when filtered by 2 μm polycarbonate (Kimfol). Because the focused electron beam anode was viewed by the XRD's at ground potential, copious quantities of ions were accelerated into the detectors. These were separated from the VUV-radiation by locating the detectors at 172 and 272 cm from the anode and utilizing time of flight discrimination or magnetic field deflection. The 25 mm diameter XRD's observed the anode through a series of baffles which allowed a 12 or 25 mm

diameter field of view. Some data were taken also with a 25 mm inside diameter cathode to allow observation of VUV-emission from the anode near the cathode. The XRD's and spectrograph viewed the pinched beam anode at 160° to the beam axis. Beam target x-radiation was viewed at 180° with a time integrated pinhole camera and as a function of radial distance, R, using silicon PIN diodes collimated to view a 5 mm diameter area of the anode.

The ions accelerated across the diode potential were observed with a Thomson mass spectrograph. This device utilizes parallel electric and magnetic fields to disperse the ions in orthogonal directions proportional to charge/energy and charge/momentum, respectively. The various charge and mass species are observed along parabolic curves at the film plane depending upon ion energy. Cross sectional views of the spectrograph are shown in Fig. 2 along with the parabolic curves for proton, deuterium, and certain carbon and aluminum charge species. Data were acquired on Kodak 101-01 film which was mounted in the spectrograph without a window. Visible emission from a corona discharge across the electric field plates severely fogged the film when hot gases from each data shot entered the spectrograph if the electric field remained on. Therefore, a thyrotron clamping circuit was used to turn off the 2.2 kV bias voltage 3 μsec after each shot. The spectrograph utilized a magnetic field of 900 G and was mounted along the electron beam diode axis with entrance aperture 20 cm from the anode.

Generator output waveforms from shot 1309 are shown in Fig. 3 which represent approximately 20 kJ of electrical energy coupled to

the diode. This pulse typically produced hemispherical craters 13 mm in diameter and 10 mm deep within 2 mm of the center of the aluminum anode. Unless denoted otherwise all data presented in the figures of this report were obtained from shot 1309. The damage pattern upon the 1 cm thick anode used for this shot is shown in Fig. 4. Collimated PIN diode data taken at R = 0 and 1 cm, shown below the electrical output data in Fig. 3, indicate that the hollow electron current sheath coalesces[8] into a focused beam at approximately 10 nsec after current initiation. The PIN diode data shown were taken on electrically similar shot 1319 because of the necessity to remove the Thomson spectrograph to acquire these data. These data, when combined with the time integrated pinhole photographs indicate a typical current density profile during the steady pinch phase of approximately

$$J(R) = 1.0\ e^{-(R/2.7\ \text{mm})^2}\ \text{MA/cm}^2, \quad R < 2.7\ \text{mm}$$

$$J(R) = 1.0\ e^{-R/2.7\ \text{mm}}\ \text{MA/cm}^2, \quad R \geq 2.7\ \text{mm}.$$

This current density profile is similar in shape to that obtained[9] on the Gamble I generator at a diode current of 0.23 MA although the absolute value is approximately twice as large because of the larger diode current used here. As with the Gamble I data no correction has been made for the ion current which could reduce the above electron current density by 10 to 20%. Corrections to the observed bremsstrahlung profile are necessary[9] when a generator is operated in negative polarity because of on-axis peaking of the bremsstrahlung. Such corrections were not made here because of the relative flatness of the

bremsstrahlung angular distribution between 140 and 180° even for low-Z targets.

The output signal from the aluminum XRD filtered by a ½ μm aluminum window is also shown in Fig. 3, time correlated with the diode electrical input and collimated PIN data. This signal is typical of those observed with a 12 mm field of view and represents approximately 1.5 J of VUV-emission between 20 and 80 eV. The signals were observed to rise slowly during the steady state pinch phase and then to jump up drastically during the impedance collapse phase. The data obtained with this filter-detector combination but with a 25 mm field of view showed little or no increase in the signal during the steady state pinch phase. However, the large signal during impedance collapse increased proportional to the area of the anode viewed and did not decay in time as rapidly when the inner edge of the cathode was viewed. These data correlate with collimated PIN data off-axis (Fig. 3) which show the late time electron beam defocusing that would indicate energy deposition near the cathode inside diameter. The XRD's filtered by 2 μm Kimfol showed only a small signal, corresponding to approximately 0.1 J between 150 and 280 eV on some shots, which also occurred when the generator voltage approached zero. This signal was quite irreproducible and therefore not considered a useful diagnostic. However, data obtained with unfiltered XRD's, which were sensitive above approximately 5 eV, show similar behavior to the data obtained with a ½ μm aluminum filter but with a much longer decay time of approximately 500 nsec. These data point out that time integrated spectrographic data taken at approximately 10 eV will be almost entirely due to the late

time interaction of the short circuit current and the plasma filling the diode.

A densitometer trace from the spectrum in the energy range from 8 to 12 eV obtained from shot 1309 is shown in Fig. 5. The spectrum contains emission and absorption lines superimposed upon the continuum. The strongest emission lines are due to carbon, nitrogen, oxygen, and silicon, which are present in the diffusion pump oil and gases absorbed upon the anode surface. The anodes were cleaned with alcohol before each data shot but were not heat treated under vacuum. Emission from three-electron ion[illegible] carbon, nitrogen and oxygen is very intense which implies a temp[illegible] to 20 eV for a plasma in thermal equilibrium. It is assumed that such ions are formed and excited in the low density region near the front of the anode plasma where electron return currents exist. The absorption spectrum is also primarily due to carbon, although lines from hydrogen, nitrogen, and oxygen appear. The spectra obtained in the energy range from 4 to 8 eV was composed almost entirely of continuum and deep absorption lines from these elements. The source of this material is not known for certain, but probably is also due to absorbed gases and hydrocarbons emitted from the anode during the primary electrical pulse. The continuum radiation falls off with increasing photon energy primarily because of the declining response of the grating near 12 eV. The grating response has not been calibrated at these energies, therefore, it is not possible to obtain a reliable limit on the temperature of the dense plasma from the continuum observed.

A limited amount of data were obtained with different atomic number anodes which indicate an increase in the continuum VUV-emission with increasing atomic number. Similar increases were observed for the signals recorded by the XRD which was filtered by $\frac{1}{2}$ μm aluminum. These observations are consistent with increased emission due to, radiation rate changes with atomic number, or the higher temperatures expected for higher atomic number anode materials. It is remarkable that thermal line radiation characteristic of the anode is essentially absent. Apparently this emission is absorbed by the anode blow-off plasma, which requires an area density of $> 10^{18}$ carbon atoms/cm^2, or the anode radiates as a blackbody. It was noted that the peak emission detected by the XRD filtered by $\frac{1}{2}$ μm aluminum (Fig. 3) was consistent in absolute magnitude with a 5 eV blackbody radiation source. This was determined by taking the product of the detector response and a 5 eV blackbody spectrum for the 12 mm diameter surface area observed.

The Thomson spectrograph data from shot 1309 are shown in Fig. 6. The data demonstrate that the primary ion current in the diode is in the form of protons. However the carbon and naturally abundant deuterium spectra can be seen when the proton signal is overexposed as in Fig. 6. The bright region of the proton spectrum is highly overexposed and indicates expansion of the collimated ion beam due to space charge effects or scattering from residual gases in the spectrograph. The device was pumped via a vacuum line which by-passed the entrance apertures but the region between apertures was evacuated only through small pump-out ports which by-passed the apertures on this shot. These ports allowed aluminum debris to enter the spectrograph

and lodge upon the film, as is evidenced by the many white spots upon the photograph in Fig. 6. This problem could be severe if a channeltron plate were used in place of the photographic film to detect the ions because even without pump-out port around the apertures some debris will pass through the apertures. The data shown in Fig. 7 were obtained with a brass anode, but without pump-out ports, and represent a clean spectra. However, approximately 6 MeV carbon 4^+ are evident because of carbon 6^+ ions which after acceleration across the diode potential have undergone charge exchange in the region between the apertures. This problem will be solved in future experiments by pumping all regions of the spectrograph with adequate lines.

The mass spectrograph data from these and other shots indicate a prevalence of carbon 3^+ and 4^+ ions. This requires an anode plasma temperature of approximately 8 eV for coronal equilibrium. This criterion would be valid at the leading edge of the anode plasma where the density is very low (approximately 10^{15} cm^{-3}) but where electric field penetration would exist and ions could be accelerated by the electric field.

An estimate of the surface temperature of the aluminum anode was also obtained, as a function of time, assuming classical absorption for a normally incident electron beam upon aluminum. This gives a lower limit to the surface temperature, because the average electron angle of incidence has been shown to be $\geq 40^{\circ}$ for a similar diode geometry[9]. The temperature was obtained from the relation

$$T(t) = \frac{F}{A}\int_{o}^{t} V(t)\ i(t)\ E(V)\ dt$$

and the calculated value is shown along with the aluminum XRD signal in Fig. 3. In this relationship F is the ratio between the temperature of the anode surface plasma and the energy absorbed per atom, here taken to be 0.1[10]; A is the area over which the electron beam is incident; V is the electron beam energy shown in Fig. 2; I is the electron current; and E is the energy absorbed, per atom, at the surface of the anode for a unit energy fluence. The value of A was taken to 1 cm^2, the equivalence of calculating the deposition at the half-maximum of the radial current profile specified above, and E was taken from published calculations[11] of the classical electron profile. The calculated temperature rises at a slow constant rate during the steady state pinch phase but very rapidly during the final stages of the electrical generator pulse when the impedance collapses. This phenomenon occurs because of the great increase in the electron stopping power with decrease in electron energy and is indicative of heating only a small amount of material very close to the surface of the anode.

The disagreements between the temperatures indicated by the absolute magnitude of XRD signal, and VUV spectrograph, and Thomson spectrograph, and the electron deposition calculation are only plus or minus factor of two and not inconsistent with a temperature variation between the surface of the anode and leading edge of the anode plasma. The calculated temperature is the lowest in value but extremely

conservative and only applies to the surface of the anode. This temperature is experimentally varified only in an indirect way by the absolute magnitude of the XRD signal. The Thomson spectrograph probes the leading edge of the anode plasma during the steady state pinch phase and gives the next highest temperature of 8 eV. Finally the time integrated VUV spectrograph samples the late time impedance collapse and the radiation from three electron carbon ions observed indicates a temperature of approximately 20 eV in a low density optically thin plasma.

It is concluded that the temperature of the anode and anode plasma varies in both space and time throughout the electron beam pulse. Since the diagnostics used cannot specify the anode or anode plasma temperature to much better than a factor of two the experimental data obtained appear consistent and indicate temperatures of a few eV. Because temperatures of many tens or hundreds of eV were not observed the electron absorption mechanism in the aluminum anode is assumed to primarily classical.

Helpful discussions with Shyke A. Goldstein, G. Cooperstein, and D. Mosher are acknowledged with pleasure.

REFERENCES

1. G. Yonas, J. W. Poukey, J. R. Freeman, K. R. Prestwich, A. J. Toepfer, M. J. Clauser, and E. H. Beckner, Proceedings of the 6th European Conference on Controlled Fusion and Plasma Physics (USSR Academy of Sciences, Moscow, 1973), p. 483.
2. J. Chang, M. J. Clauser, J. R. Freeman, G. R. Hadley, J. A. Halbeib, D. L. Johnson, J. G. Kelly, G. W. Kuswa, T. H. Martin, P. A. Miller, L. P. Mix, F. C. Perry, J. W. Poukey, K. R. Prestwich, S. L. Slope, D. L. Swain, A. J. Toepfer, W. H. VanDevender, M. M. Widner, T. P. Wright, and G. Yonas, Sandia Laboratories Report No. SLA 74-5176, 1974 (unpublished).
3. L. I. Rudakov and A. A. Smarsky, in Ref. 1, p. 487.
4. F. Winterberg, Phys. Rev. 174, 212 (1968); Nucl. Fusion 12, 353 (1972).
5. F. C. Perry and M. M. Widner, J. Appl. Phys. 47, 127 (1976).
6. L. S. Levine and I. M. Vitkovitsky, IEEE Trans. Nucl. Sci. 18, 4, 225 (1974).
7. J. R. Kerns and D. J. Johnson, J. Appl. Phys. 45, 5225 (1974).
8. A. E. Blaugrund and G. Cooperstein, Phys. Rev. Lett. 34, 461 (1975).
9. D. J. Johnson and Shyke A. Goldstein (to be published).
10. D. Mosher, Phys. Rev. A10, 2330 (1974).
11. I. V. Spencer, National Bureau of Standards Monograph 1, 1959 (unpublished).

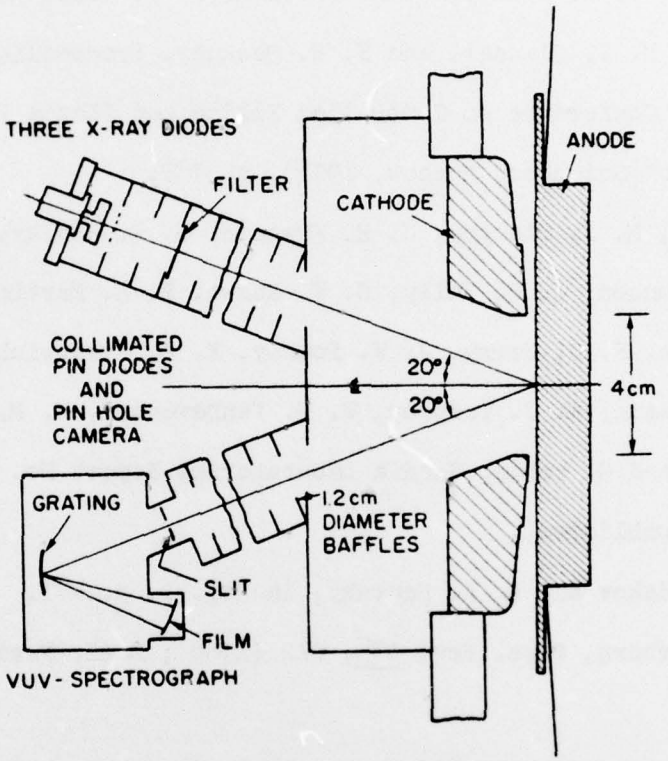

Fig. 1 — Schematic of the apparatus

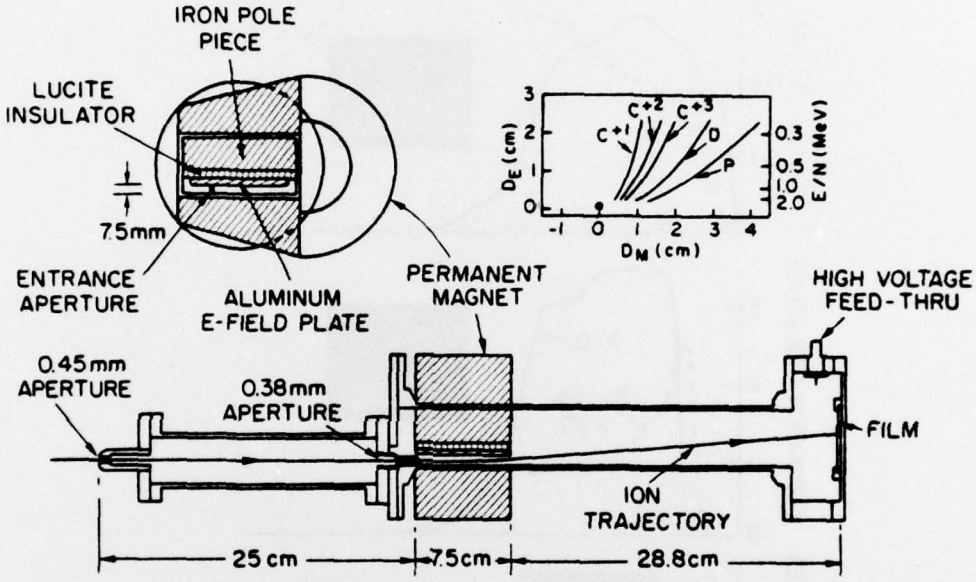

Fig. 2 — Cross-sectional views of the Thomson mass spectrograph and a plot of the parabolic dispersion curves for various ion species

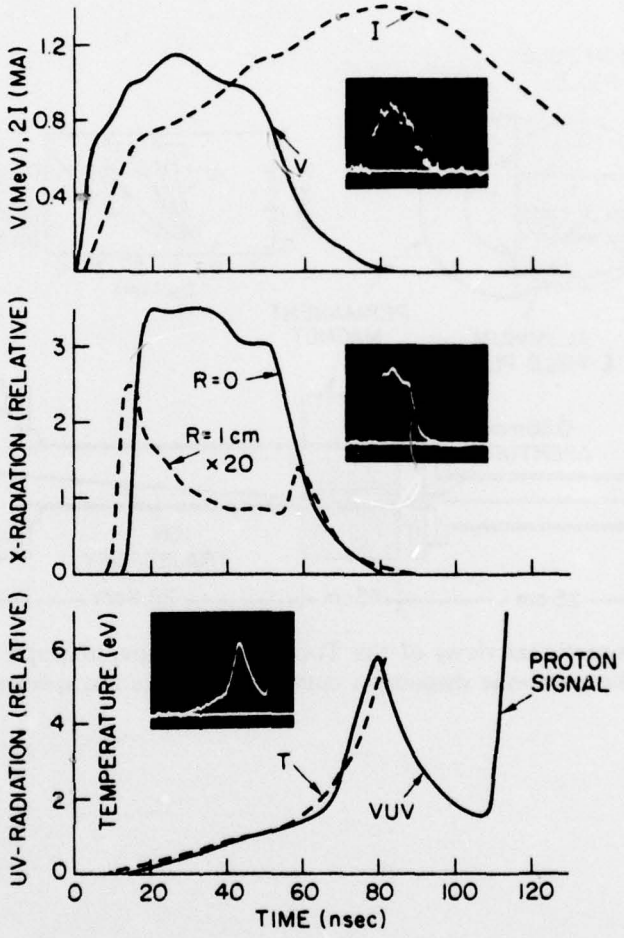

Fig. 3 — (Top) Diode voltage (V) and current (I) from shot 1309. The voltage has been corrected for inductive contribution. (Center) Measured x-radiation signals for shot 1319 from collimated PIN diodes observing a 5 mm diameter area of the anode at r = 0 and 1 cm. (Bottom) Observed signal for shot 1309 from an aluminum XRD filtered by 1/2 μm aluminum which views a 1.2 cm diameter area in the center of the anode. The dashed curve represents a calculated anode surface temperature for the measured electron beam parameters, assuming normally incident electrons, classically absorbed by a 1 cm diameter aluminum target.

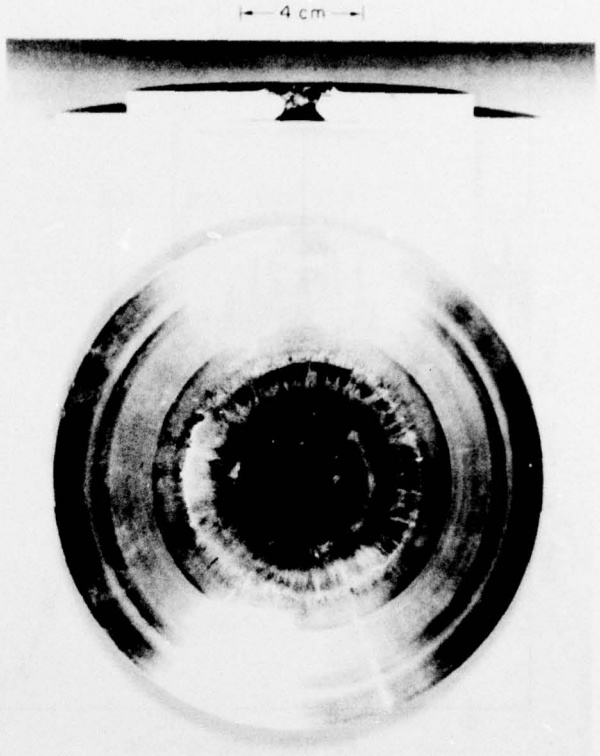

Fig. 4 — Aluminum anode from shot 1309

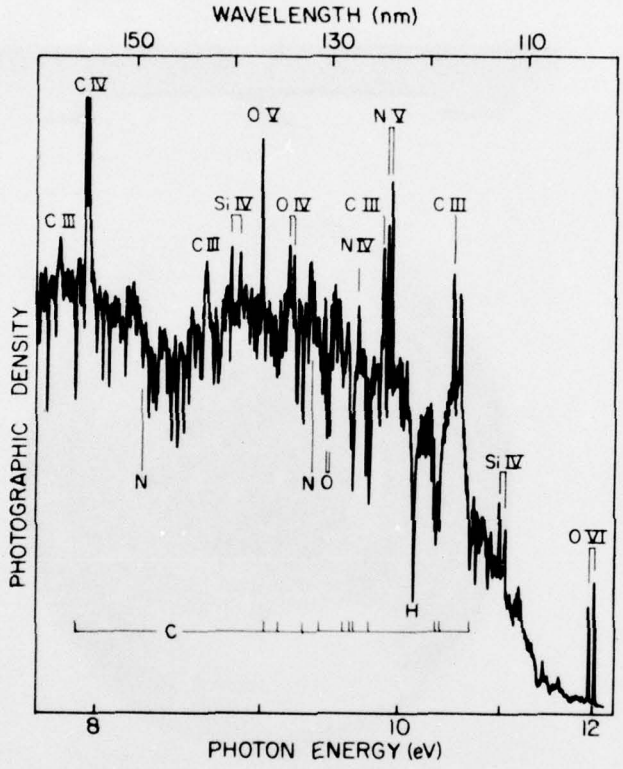

Fig. 5 — Densitometer trace of the spectrum obtained from shot 1309. Emission lines are from the ions indicated above the trace. Some absorption lines for ground state atoms are identified below the trace.

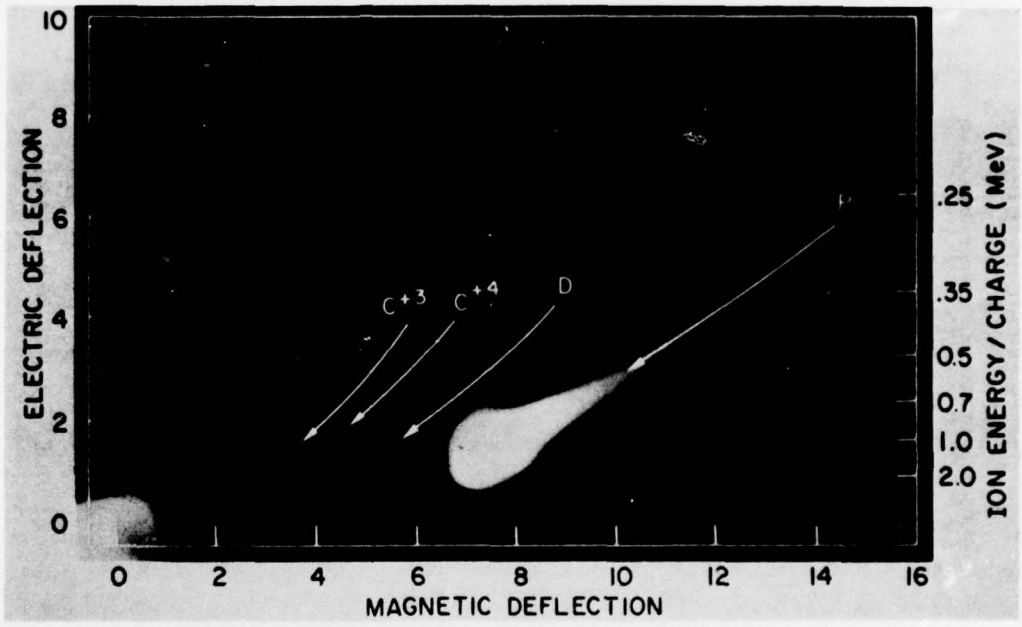

Fig. 6 — The Thomson mass spectrograph data from shot 1309

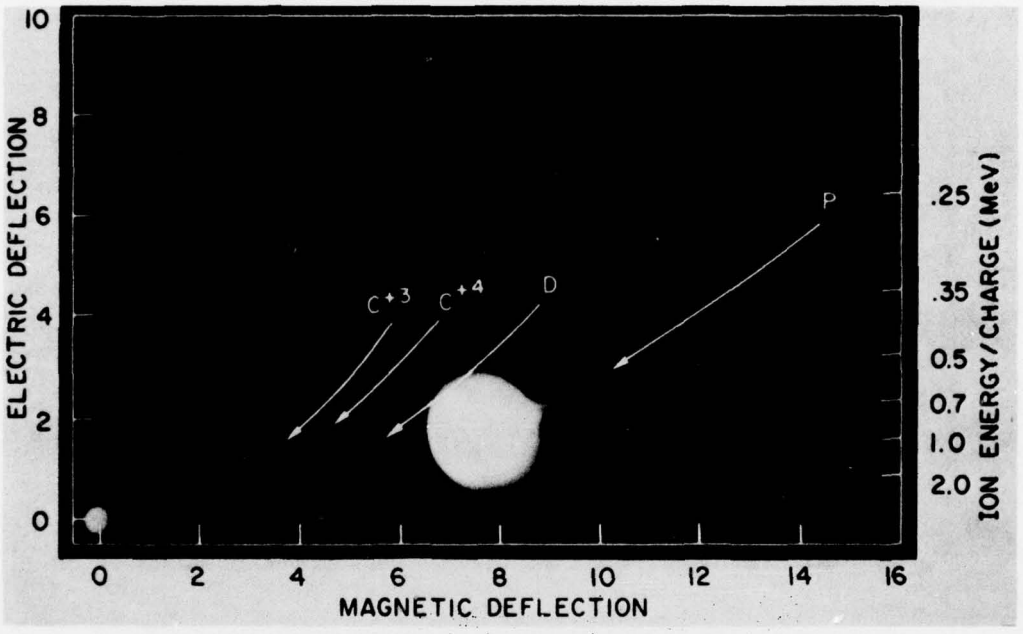

Fig. 7 — The Thomson mass spectrograph data from shot 1317 obtained with a brass anode

DISTRIBUTION LIST

1. Director
Defense Advanced Research Projects Agency
Architect Building
1400 Wilson Boulevard
Arlington, Virginia 22209
Attn: LTC R. P. Sullivan

2. Director
Defense Nuclear Agency
Washington, D. C. 20305
Attn: DDST, Mr. Peter Haas
RATN
STTL, Technical Library (2 copies)
RAEV (2 copies)
STVL
STSI

3. Commander
Field Command
Defense Nuclear Agency
Albuquerque
Kirtland AFB, New Mexico 87115
Attn: FCPR

4. Chief
Field Command
Defense Nuclear Agency
Livermore Division
Box 808
Livermore, California 94550
Attn: FCPR-L

5. Director
Defense Research and Engineering
Washington, D. C. 20301
Attn: DAD (SK) Mr. G. R. Barse

6. Commander
Harry Diamond Laboratories
Adelphi, Maryland 20783
Attn: AMXDO-RBF, Mr. John Rosado
AMXDO-RBH, Mr. S. Graybill
AMXDO-RC, Dr. Robert Oswald, Chief, LAB 300

7. Air Force Weapons Laboratory, AFSC
Kirtland AFB, New Mexico 87117
Attn: DY, Dr. Guenther
EL, Mr. John Darrah
DYS, Dr. Baker
SAA
SUL, Technical Library
ELP, TREE Section

8. Space and Missile Systems Organization
Post Office Box 92960
Worldway Postal Center
Los Angeles, California 90009
Attn: SKT, Mr. Peter H. Stadler
RSP, System Defense and Assessment, LTC Gilbert

9. Sandia Laboratories
P. O. Box 5800
Albuquerque, New Mexico 87115
Attn: Document Control for 5220, Dr. J. V. Walker
Document Control for 5242, Dr. G. Yonas
Document Control for Technical Library

10. Aerospace Corporation
P. O. Box 92957
Los Angeles, California 90009
Attn: Mr. J. Benveniste
Dr. Gerald G. Comisar, Jr.

11. University of Texas
Fusion Research Center
Physics Building 330
Austin, Texas 78712
Attn: Dr. William E. Drummond

12. Battelle Memorial Institute
Columbus Laboratories
505 King Avenue
Columbus, Ohio 43201
Attn: Mr. P. Malozzi

13. Maxwell Laboratories, Inc.
9244 Balboa Avenue
San Diego, California 92123
Attn: Dr. P. Korn

14. Mission Research Corporation
735 State Street
Santa Barbara, California 93101
Attn: Dr. Conrad L. Longmire

15. Physics International Corporation
2700 Merced Street
San Leandro, California 94577
Attn: Document Control for Dr. Sidney Putnam
Document Control for Mr. Ian Smith

16. R & D Associates
P. O. Box 9695
Marina del Rey, California 90291
Attn: Dr. Bruce Hartenbaum

17. Science Applications, Inc.
P. O. Box 2351
La Jolla, California 92037
Attn: Dr. J. Robert Beyster

18. Stanford Research Institute
333 Ravenswood Avenue
Menlo Park, California 94025
Attn: Dr. Robert A. Armistead, Jr.

19. Dr. Victor A. J. Van Lint
Mission Research Corporation
7650 Convoy Court
San Diego, California 92111

20. Commander
Naval Surface Weapons Center
White Oak Laboratory
Silver Spring, Maryland 20910

21. DASIAC, GE Tempo
El Paseo Building
816 State Street
Santa Barbara, California 93102

22. DDC (2 copies)

23. Code 2628 (20 copies)

24. Code 7700

25. Code 7770 (20 copies)